Advances in Water Resources 211 (2026) 105253

Contents lists available at ScienceDirect

Advances in Water Resources

journal homepage: www.elsevier.com/locate/advwatres

Evaluation of the Iberian barbel resting behavior in vertical slot fishways: A two-dimensional Eulerian Lagrangian Agent based approach

M.X. Ruiz-Coello [a,*], F.J. Sanz-Ronda [a], A. Bottacin-Busolin [b], J.F. Fuentes-Pérez [a]

[a] Group of Applied Ecohydraulics, Department of Agricultural and Forest Engineering, Sustainable Forest Management Research Institute, Universidad de Valladolid, ETSIIAA, Avenida de Madrid 44, Campus La Yutera, 34004 Palencia, Spain
[b] Department of Industrial Engineering, University of Padua, Italy

ARTICLE INFO

Keywords:
Ascent ability
ELAM
IBM
Iberian barbel
Passage efficiency
Resting behavior
TELEMAC-2D
VSF

ABSTRACT

Fishways design requires careful evaluation of hydraulic and biological requirements. This study presents a Eulerian-Lagrangian Agent Based Model of fish migration through Vertical Slot Fishways which relies on 2D flow simulations. The model, provided as a Python toolbox named t-ELAM-acPy_2D, integrates two-dimensional flow fields with an agent-based description of fish movement and behavior. t-ELAM-acPy_2D represents fish upstream movement using multiple behavioral states, including resting responses, a key element for cyprinid movement. The model also performs an energy-expenditure analysis, using a real-time, dynamic flow field. It was calibrated and validated across different fishway configurations, using Iberian barbel (*Luciobarbus bocagei*) as fish targeted species. The model successfully reproduced fish habitat spatial distribution, ascent times and, to a limited extent, passage efficiency. The results show that the toolbox can efficiently support design, optimization, and evaluation of different fishway configurations.

Symbols and abbreviations

h	water depth
u_i	velocity component
t	time
Z	free surface elevation
x_i	cartesian axis
S_f	friction source term
g	gravity acceleration
ν_t	turbulent viscosity
ΔE	energy spent in a time step
Δt	time step
ρ	water density
C_D	fish drag coefficient
Δt_{ELAM}	time step IBM
k	turbulent kinetic energy
:	turbulent dissipation rate
C_μ, $C_{\varepsilon 1}$, $C_{\varepsilon 2}$	constants $k-\varepsilon$ model
σ_k, σ_ε	constants $k-\varepsilon$ model
S_{ij}	strain rate tensor
BL	fish body length
VSF	vertical slot fishways
S	wetted surface of the agent
u_{flow}	flow speed
u_P	agents' relative velocity
T_f	time to fatigue
D_{max}	distance to be covered
$p(\Phi)$	gaussian probability
Φ	hydrodynamic variable IBM
σ	standard deviation of Φ
μ	mean of Φ
W	weight of Φ for P
P	joint probability
β_i	logistic model constants
τ_{xy}	Reynolds shear stress
P_{pass}	passage proportion
u_{fish}	fish swimming speed
Ω	entire domain
Ω_{ELAM}	domain IBM

1. Introduction

Anthropogenic development has affected the free flowing of rivers. Only 37% of large rivers persist untouched worldwide (Grill et al.,

* Corresponding author.
E-mail address: marcelo.ruiz@uva.es (M.X. Ruiz-Coello).

https://doi.org/10.1016/j.advwatres.2026.105253
Received 19 December 2025; Received in revised form 18 February 2026; Accepted 18 February 2026
Available online 19 February 2026

2019). European rivers are probably the most affected in the world, within only one third of the rivers length remaining in good status (Grizzetti et al., 2017). At least 1.2 million barriers in 36 countries in Europe impact river connectivity (Belletti et al., 2020). Central Europe's barrier density is the highest, while the Balkans and Baltic regions are the lowest. More than 187000 barriers have been estimated to be placed in the rivers of the Iberian Peninsula (Belletti et al., 2020). This largely affects the normal interaction of riverine ecosystem fluxes. In the communication to the European Parliament (European Commission, 2020). The European Commission presented the EU Nature Restoration Plan, which seeks to restore freshwater ecosystems by removing and adjusting barriers that impact fish migration. In order to achieve this objective, it is necessary to restore 25000 km of rivers by 2030. Fishways are the most common structural measure to restore river connectivity. However, to date, they are considered as a mitigation measure rather than a solution (Silva et al., 2018).

Vertical Slot Fishways (VSF) are one of the most extended types of fish passing structure worldwide (Fuentes-Pérez et al., 2017). In the most recent meta-analysis on the efficiency of fishways, Hershey (2021) displayed for VSFs a passage efficiency, defined as the ratio between the number of fish detected beyond the fishway exit and the number of fish recorded at or within the fishway entrance, of 0.63. In a more species focused study, Bravo-Córdoba et al., (2021) conducted a systematic review on VSFs in the Iberian peninsula assessing the fish passage of the Iberian Barbel (*Luciusbarbus bocagei*), Nase (*Pseudochondrostoma polylepis*) and Brown Trout (*Salmo trutta*). They observed that VSF displayed a median passage efficiency of 0.71 ranging from 0.68 to 0.96, mainly influenced by hydraulic conditions and fish size and species. Still, the desired efficiency, higher than 0.90 (Lucas and Baras, 2001), to recover river connectivity and fish migration normal fluxes is barely achieved. Both biological and physical aspects of fish passage structures need to be addressed to guarantee passage efficiency (Silva et al., 2018).

There are still multiple unknowns in VSF performance and a diverse range of efficiencies in different studies (Bunt et al., 2012; Hershey, 2021). This has pushed for the performance of biological evaluations of fishways after these structures are constructed, as there is not a single tool that can accurately predict spatial occurrence distribution, ascent time, or passage efficiency. Eulerian Lagrange Agent based Models (ELAMs) raise as be a suitable approach to explore passage efficiency and fish migration paths to assess new fishways designs. First developed by Goodwin et al. (2006) to evaluate fish downstream migration pathways, it has been recently applied in the evaluation of fish migration pathways in VSF (Gao et al., 2016; Kulić et al., 2021; Tan et al., 2018). Despite the fact that in some studies energy expenditure has been addressed (Kulić et al., 2021; Ruiz-Coello et al., 2024a; Tan et al., 2022), biological indicators such as fatigue, exhaustion, or passage success probability have been disregarded. Nowadays, significant work has been performed in the empirical evaluation of these indicators (Bravo-Córdoba et al., 2021, 2018; Sanz-Ronda et al., 2019, 2015), and its potential applicability has not been considered yet.

The aim of this study is to evaluate the inclusion of a "Resting Behavior (B_R)" of the Iberian Barbel (*Luciobarbus bocagei*) in a dynamic ELAM (t-ELAM-acPy_2D) to predict the ascent transit time and passage efficiency of VSF complex geometries. To the knowledge of the authors, this behavior has not been addressed in similar approaches before. In addition and contrary to previous ELAM implementations (Gao et al., 2016; Ruiz-Coello et al., 2024a; Tan et al., 2018), the model presented in this manuscript relies on a real time 2D hydrodynamic model outcome to drive agent's behavior (Ruiz-Coello et al., 2024b). To implement the ELAM, the Application Programing Interface (API) TelAPy included in the TELEMAC-2D distribution (Electricité de France et al., 2021; Goeury et al., 2022) was used. For this purpose, our study proposes an ELAM-based tool that (1) incorporates resting behavior, as observed in real fishway experiments; (2) adapts to unsteady, non-uniform flow conditions; and (3) accounts for the inherent randomness of fish cognitive responses. In addition, our study covers the assessment of the energy cost and passage proportion. To this end, three different cases of study were evaluated. First, a simple geometry for which laboratory data are available was considered as a base line for the implementation and calibration of the model. Subsequently, two different VSF geometries were used as a validation of ascent times and passage proportion.

2. Materials and methods

2.1. Experimental data

The targeted fish species to calibrate and test the ELAM model is the Iberian barbel (*Luciobarbus bocagei* Steindachner, 1864). Iberian barbel is endemic from the northwest of the Iberian Peninsula and one of the most common fish species in that region (Freyhof and Kottelat, 2008). Barbels are rheophilic cyprinids that display migratory behavior with reproductive and overwinter movements from spring to late autumn.

To develop the ELAM model (Fig. 1) we used three different VSF configurations. The VSF configuration 1, VSF_1, corresponds to a full-scale model of the design 11 from Rajaratnam et al. (1992). It is, located at the Hydraulics and Environment Department of the National Laboratory for Civil Engineering (LNEC), in Lisbon, Portugal. Studies conducted on this VSF model explored both the success and passage times for Iberian barbel (Romão et al., 2017), as well as their spatial preferences under various hydrodynamic scenarios (Fuentes-Pérez et al., 2018). It is noteworthy that barbels showed a preference for areas within the pools that were surrounded by walls, such as corners, and the hydrodynamic scenario significantly affected the pool usage. This data contributed to the calibration and validation of the ELAM standard, as it helped to establish a correlation between hydrodynamic variables and spatial preference.

On the other hand, experimental data on ascent time from Sanz-Ronda et al. (2019, 2016) were used to validate the Resting Behavior, B_R. (Sanz-Ronda et al., 2019) pit-tagged Southern Iberian barbels (*Luciobarbus sclateri* (Günther, 1868)); a congener with similar morphology and swimming behavior to Iberian barbel to evaluate the efficiency and ascent time of a VSF located in the Segura River Basin (Southeast of Spain), VSF_2. Sanz-Ronda et al. (2016), in the same line, pit-tagged Iberian barbels and tested them in three different flow scenarios, 0.245, 0.334 and 0.402 m/s^3 for low, medium, and high discharge, respectively, to evaluate the fish ascent times in a VSF located at the Porma River at the Duero River Basin (Northwestern Spain), VSF_3. Both VSF_1 configurations, VSF_2 and VSF_3, are based on the design 1 from Rajaratnam et al. (1992).

2.2. Hydrodynamic evaluation

The individual based model presented in this paper is coupled with TELAMAC-2D. Considering that the base model developed by Ruiz-Coello et al., (2024a, 2024b) uses 3D simulations as input, we performed the calibration alongside OpenFOAM 3D simulations to determine the bias of the depth-averaged flow assumption on the coefficients of the Individual Based Model (IBM). Details on the numerical set up of 3D simulations can be found in their publication. TELEMAC-2D comes as part of the TELEMAC open-source software (Electricité de France et al., 2021). It solves the 2D shallow water equations or 2D Saint Venant Equations (Eq. 1) with the finite element approach:

$$\frac{\partial h}{\partial t} + \frac{\partial (h u_i)}{\partial x_i} = 0 \tag{1a}$$

$$\frac{\partial u_i}{\partial t} + u_j \frac{\partial u_i}{\partial x_j} = -g \frac{\partial Z}{\partial x_i} + S_f + \frac{1}{h} \frac{\partial}{\partial x_j} \left(2\, h\, \nu_t\, S_{ij}\right) \tag{1b}$$

where $i, j = 1, 2$, h is water depth, u_i is the velocity component, g is the gravitational acceleration, Z is the free surface elevation, ν_t is the turbulent diffusion coefficient (turbulent viscosity), S_f is the source term

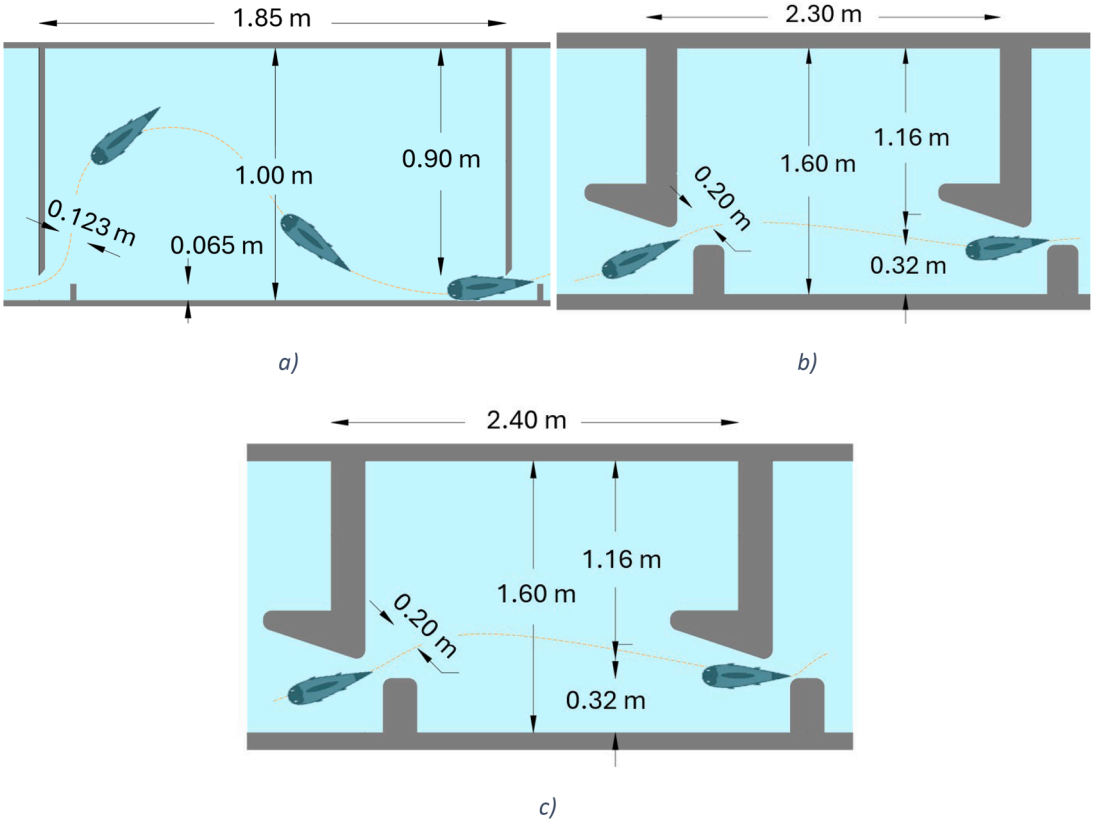

Fig. 1. Geometry configurations of the VSF from a) VSF_1 (Romão et al., 2017), b)VSF_2 (Sanz-Ronda et al., 2019) and c) VSF_3 (Sanz-Ronda et al., 2016). Upstream is at the left and downstream is at the right. Schematic fish are swimming upstream.

due to friction and S_{ij} is the strain rate tensor. Manning's coefficient was kept in 0.03 $s/m^{1/3}$; however, from previous studies (Ruiz-Coello et al., 2024c) small variations do not care large changes in hydrodynamics of VSF. Turbulent diffusion coefficient is modeled using the k- ε model variation for shallow water equations (Rastogi and Rodi, 1978).

$$\frac{\partial k}{\partial t} + u_i \frac{\partial k}{\partial x_i} = \frac{1}{h}\frac{\partial}{\partial x_j}\left(h \frac{\nu_t}{\sigma_k}\frac{\partial k}{\partial x_j}\right) + 2\,\nu_t\, S_{ij}\, S_{ij} - \varepsilon + P_{kv} \tag{2a}$$

$$\frac{\partial \varepsilon}{\partial t} + u_i \frac{\partial \varepsilon}{\partial x_i} = \frac{1}{h}\frac{\partial}{\partial x_j}\left(h \frac{\nu_t}{\sigma_\varepsilon}\frac{\partial \varepsilon}{\partial x_j}\right) + \frac{\varepsilon}{k}\left[C_{1\varepsilon}\,\left(2\,\nu_t\, S_{ij}\, S_{ij}\right) - C_{2\varepsilon}\,\varepsilon\right] + P_{\varepsilon v} \tag{2b}$$

$$\nu_t = C_\mu \frac{k^2}{\varepsilon} \tag{3}$$

$$S_{ij} = \frac{1}{2}\left(\frac{\partial u_i}{\partial x_j} + \frac{\partial u_j}{\partial x_i}\right) \tag{4}$$

Where k and ε are the turbulent kinetic energy and its dissipation, respectively. The terms P_{kv} and $P_{\varepsilon v}$ are bed related source terms, which in this case are 0. The terms σ_k, σ_ε, $c_{1\varepsilon}$, $c_{2\varepsilon}$ and c_μ are empirical coefficients, whose values are 1.0, 1.31, 1.44, 1.92 and 0.09, respectively. Our models consider only two open boundaries, inflow and outflow. Solid boundaries are defined as no mass flux located in the lateral walls of the channel (Fernandes et al., 2001). The model solves a first order temporal Euler explicit scheme and non-structured grid first order upwind scheme. Spatial discretization of the geometry evaluates 28274 elements for VSF_1, 22494 elements for VSF_2, and 22959 elements VSF_3. Previously, both grid convergence analysis and the impact of the Manning's coefficient were undertaken (Ruiz-Coello et al., 2024c). The convergence was achieved at cell size, Δx, in [2.9, 4.0] cm.

Two – dimensional models, in spite of overestimating turbulent variables (Chorda et al., 2010; Ruiz-Coello et al., 2024c), have been shown to effectively reproduce the hydraulics of VSF (Bombač et al., 2017; Cea et al., 2007; Puertas et al., 2012). The standard IBM is the one developed by Ruiz-Coello et al., (2024a), and the additional resting behavior is based on the experimental observations of Fuentes-Pérez et al. (2018).

2.3. Individual based model

Our development works with the IBM behavioral rules presented by Ruiz-Coello et al., (2024a). The model includes upstream migration and wall avoidance whose input is the nodes of an unstructured grid, in this case in TELEMAC-2D. In addition, our development includes a resting behavior which aims to represent the time taken by the barbels to energy recovery while swimming upstream in a VSF.

Fish sensory systems are sensitive to velocity changes for frequencies below 50 Hz (McHenry and Liao, 2014). Therefore, the time step for the IBM simulations was set to 0.25 seconds and the time of simulation was the total recording time for each VSF presented in this manuscript. The IBM time step is much higher than those observed in the hydrodynamic simulations, 1.0 e -04 s and 1.0 e -03 s, for 3D and 2D, respectively. The maximum courant number was 0.8.

2.3.1. Upstream migration

In the base IBM, the approach implemented by Gao et al. (2016) and Tan et al. (2018) was considered. However, a stochastic variable to add randomness to the path selection was implemented. Finally, they implemented escaping behavior from high velocity zones in upstream migration paths governed by the following equations:

$$p(\Phi) = \frac{1}{\sigma\sqrt{2\pi}} e^{-\frac{1}{2}\left(\frac{\Phi-\mu}{\sigma}\right)^2} \tag{5}$$

$$P = \sum W \cdot p(\Phi) \quad (6)$$

where $p(\Phi)$ is the normal distribution linked to the hydrodynamic variable Φ, μ is mean of the normal distribution, σ is the standard deviation, P is the joint probability or the likelihood of a node in the grid to be chosen for the agent in the next step, W is the weight of influence of each variable Φ. The hydrodynamic variables considered are turbulent kinetic energy, k, velocity magnitude, $|u_j|$, and velocity strain rate, S_{ij}. This evaluation is undertaken in the sensory circle of influence (Gao et al., 2016; Goodwin et al., 2006).

In this behavior the agent considers only the upstream domain of the sensory scope as presented in Ruiz-Coello et al., (2024a) and Tan et al. (2018). As in the initial development, the agent will swim towards the chosen position randomly using the critical swimming speed, u_{crit}, and bursting swimming speed, u_{burst}, in the slot zone. These parameters were taken from the study of Ruiz-Legazpi et al. (2018) and Sanz-Ronda et al. (2015). Bursting speed was defined from 15 BL/s to 25 BL/s, whereas the critical swimming speed was set to 5 BL/s to 15 BL/s, where BL is the fish Body Length. Random path selection seeks to address internal and external factors, such as light, noise, stress, among others, that influence fish path selection, but cannot be explicitly computed.

2.3.2. Wall avoidance

As presented by Ruiz-Coello et al., (2024a), when the agent finds a wall node, the agent seeks to avoid the wall instead of jumping it. The behavior is a combination of the upstream migration behavior described above and the attraction to the jet zone. Contrary to the upstream migration behavior, this behavior considers all the sensory scope for choosing the path.

2.3.3. Resting behavior

The description of this exploratory behavior was based on the data collected by (Fuentes-Pérez et al., 2018). They considered three scenarios to evaluate fish spatial distribution within a fishway pool decomposed in 125 blocks and performed statistical modeling using a Poisson distribution. To complement their analysis, we performed a similar statistical modeling, Generalized Linear Model (GLM) Logistic Regression, considering the variable "Walls", which represent the number of surrounding walls in each of the blocks in the pool, 1, 2 or 3, as categorical type. Finally, the variable "Scenarios", considered in the experimental analysis, was neglected. In the experiment, it was observed that Iberian Barbels preferred blocks which were surrounded by three walls. Experimental data on habitat preference was measured in 1 frame per second (around 1,400 counts per scenario) in 125 blocks in the fifth pool of the experiment. For more information on the experimental data refer to Fuentes-Pérez et al. (2018). As can be seen in Fig. 2, most of the counts are concentrated in a single block in each scenario. Therefore, considering that only 4 out of 125 blocks are surrounded by 3 walls, the statistical modelling we conducted considered two sets of coefficients, one to predict the peaks in the corners and the other to model the rest of the pool (Fig. 2). Table 1 shows the coefficients of the GLM Logistic Regression.

$$\ln(Y) = \beta_0 + \beta_1 X_1 + \beta_2 X_2 + \ldots + \beta_n X_n \quad (7)$$

Since all the hydrodynamic variables can be extracted from hydrodynamic simulation. In each node the number of counts Y is computed.

Table 1
The first GLM logistic regression formula represents the peaks, i.e., the predicted counts in the corner zones, where Fuentes-Pérez et al. (2018) registered the maximum values. The second GLM logistic regression formula represents the normal values of the predicted counts, out of the corners.

$= \beta_0 + \sum_{i=1}^{3} \beta_i\ Wall_i + \beta_4\ k + \beta_5\ |u_j| + \beta_6\ k\ |u_j| + \sum_{i=7}^{9} \beta_i\ Wall_i \tau_{xy}$ $R^2 = 0.58$, Err = 433

i	Variable	βi	std-error	z - score	p>|z|
0	Intercept	1.4046	0.116	12.061	0.000
1	Wall = 1	1.6248	0.117	13.889	0.000
2	Wall = 2	2.8791	0.118	24.325	0.000
3	Wall = 3	4.1886	0.120	35.048	0.000
4	k	-5.5953	1.117	-5.011	0.000
5	$\|u_j\|$	-3.5894	0.202	-17.787	0.000
6	$k\|u_j\|$	16.5923	2.096	7.916	0.000
7	(Wall = 1)* τ_{xy}	0.0525	0.008	6.192	0.000
8	(Wall = 2)* τ_{xy}	0.0828	0.007	12.543	0.000
9	(Wall = 3)* τ_{xy}	0.4112	0.014	30.059	0.000

$\ln(Y) = \beta_0 + \sum_{i=1}^{3} \beta_i\ Wall_i + \beta_4\ k + \beta_5\ |u_j| + \beta_6\ k\ |u_j|$ $R^2 = 0.22$, Err = 403

i	Variable	βi	std-error	z-score	p>|z|
0	Intercept	1.3307	0.117	11.350	0.000
1	Wall = 1	1.3730	0.113	12.196	0.000
2	Wall = 2	2.5844	0.113	22.867	0.000
3	Wall = 3	3.9891	0.113	35.303	0.000
4	k	-6.7893	1.283	-5.293	0.000
5	$\|u_j\|$	-1.6342	0.209	-7.837	0.000
6	$k\|u_j\|$	7.5611	2.684	2.817	0.005

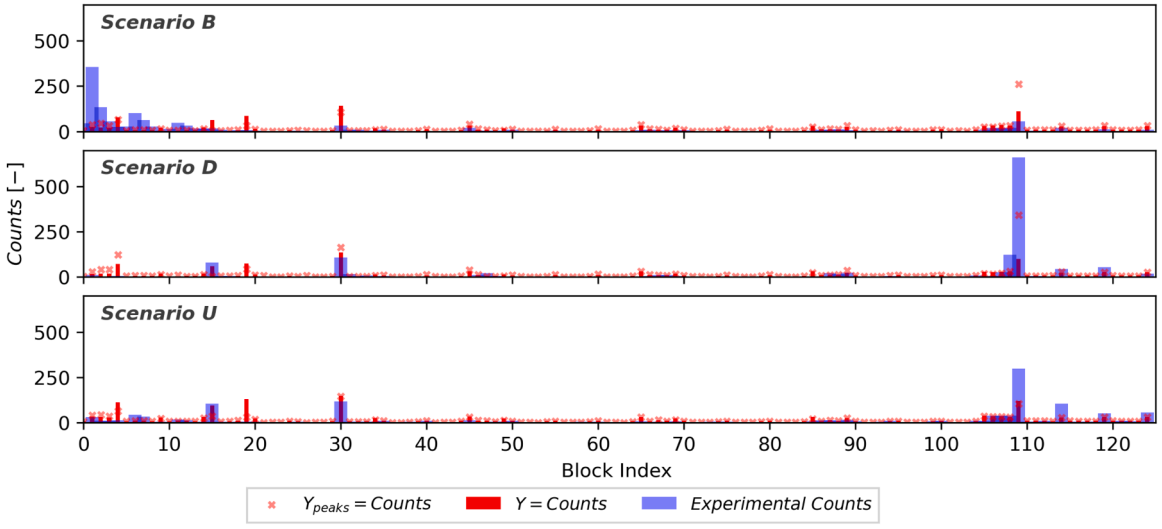

Fig. 2. Modelled (red bars Y & and cross scatter Y_{peaks}) and observed (blue bars) iberian barbel spatial preferences. Three scenarios from Fuentes-Pérez et al. (2018), Backwater profile (B), Drawdown profile (D) and (U) uniform profile. Predictions in the peaks suit well the experimental measurements in scenarios D and U whose peaks are in block 110, while in scenario B the peak is in block 2. Besides the peaks, Model Y does not largely differ from Y_{peaks} in every scenario.

The nodes which are closer to a wall will compute the counts as the maximum between the functions found, $Y = \max(Y, Y_{peaks})$. The agent will randomly choose between the 50% of the highest values contained in the sensory sphere (Gao et al., 2016; Ruiz-Coello et al., 2024a, 2024b; Tan et al., 2018). The agent will approach the position chosen with a channel ground speed (Sanz-Ronda et al., 2015), u_{ground}, set from 1.5 BL/s to 6.1 BL/s (randomly selected). Once stated the action, the triggering impulse was also defined. The impulse is linked to the time to fatigue, T_f, as a function of the fish swimming speed, u_{fish} (Fig. 3). This parameter is defined based on the swimming actions of the fish and is decreasing in time, when it reaches down to zero, the behavior is triggered.

$$T_f = e^{3.33-0.083*\ u_{fish}};\ if\ u_{fish} \geq 15\ BL \tag{8}$$

$$T_f = e^{5.47-0.202*\ u_{fish}};\ if\ u_{fish} < 15\ BL \tag{9}$$

Based on the experimental data, fish velocity was computed at each time step on the assumption that fish was resting. Thus, fish swimming speed, u_{fish}, was calculated according to the proposal from Sanz-Ronda et al. (2015) assuming that T_f was higher than 100 seconds for u_{fish} lower than 5 BL/s.

2.4. Calibration

The calibration was performed following three stages, hydrodynamic simulations, standard ELAM, and resting behavior. The numerical and physical parameters used in the hydraulic simulation for both, two-dimensional and three-dimensional, approaches were the same as the ones presented in the results of Ruiz-Coello et al. (2024c). They performed a grid convergence analysis in 3D and 2D simulations for VSF hydrodynamic simulations with mild and steep slopes. Changes in roughness while essential for two-dimensional approaches were found to be not relevant in simulations of VSF. In this study, three – dimensional and two-dimensional hydrodynamic simulations were validated mostly by comparison of water level distribution as shown in Fig. 4.

Additionally, flow topology was evaluated. In Fig. 5, flow velocities are presented. Flow topology was better captured by the three-dimensional simulations. Simulated velocity magnitudes are similar to those measured in laboratory. These results agree with those presented by Ruiz-Coello et al. (2024c).

After hydrodynamic calibration, IBM was calibrated. The calibration methodology for the IBM can be more explored in the study of Ruiz-Coello et al. (2024a). Contrary to their approach, the comparison parameter was the spatial preferences observed in VSF_1, i.e., the proportion of the time spent by the Iberian barbel in each block of the pool. This was evaluated as frequency of use, $FU = counts_i/\sum counts$ for both the barbel and the agent. At this stage, only the IBM was simulated at the fifth pool of the fishway with the results of the Eulerian simulations. Fifteen thousand IBM simulations were undertaken in 2D (2384 nodes) and 1000 simulations in 3D (669300 nodes) due to computational constraints. The objective function was the minimization of the Mean Absolute Error of *FU*. Ruiz-Coello et al. (2024b) concluded that despite that shallow water equations simulation outcome serves as a suitable input in ELAM models, the influence of some hydrodynamic variables can be biased from what fish experience. Therefore, to assess this bias and to generalize the model, both approaches, 2D and 3D, were considered. In addition to their study, resting behavior (Poisson distribution) was included into the Probability Density Functions of upstream migration (Gaussian distribution).

Finally, the resting behavior triggering parameters were also evaluated. With the data set built from the calibration the zone of the pool in which the resting behavior should be triggered along with the uncertainty of the triggering zone, were included. This was performed comparing in which zone of the pools the resting behavior was triggered, and with a frequency analysis to estimate the probability. Due to the measurements available, only VSF_1 was used for the calibration of the model, while VSF_2 and VSF_3 were used for validation. Validation was qualitatively assessed contrasting the median of ascent times across all VSF configurations. This final ELAM, with the resting behavior, was only implemented in two-dimensional framework, since the total IBM simulation time increased between 29 to 40 times at least for 2D simulations. Thus, 3D simulations were unfeasible.

2.5. Energy assessment and passage proportion

As an added value and only for data analysis, t-ELAM-acPy_2D computes the energy cost and the passage proportion of the agents at each time step. The energy cost is computed from the drag power experienced by the agent. Swimming energetics is liked to anaerobic activity, ranging from gentle sustained periods of swimming to sudden brief bursting events. Inertial forces or pressure drag can return the energy cost of fish swimming (McKenzie, 2011). Consistently, the overall energy loss per unit of time or drag power is given by:

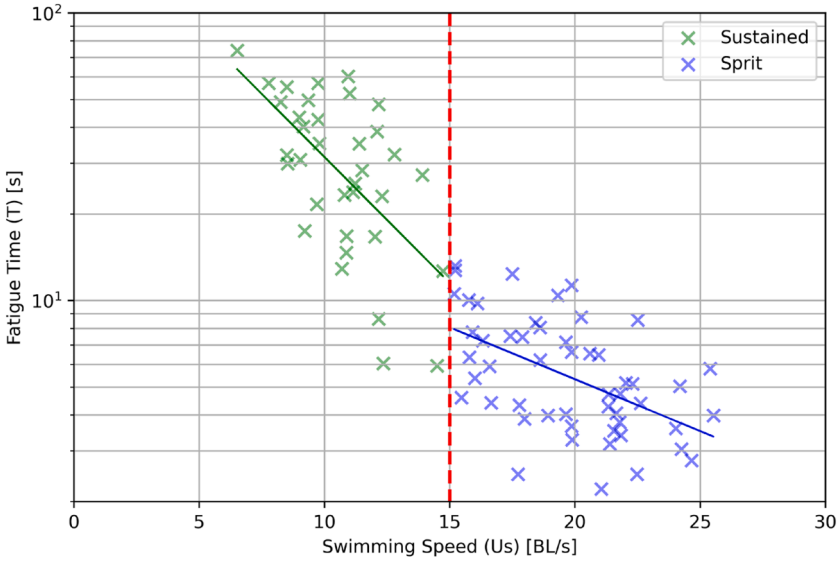

Fig. 3. Relationship between swimming speed and fatigue time for the Iberian Barbel (Sanz-Ronda et al., 2015).

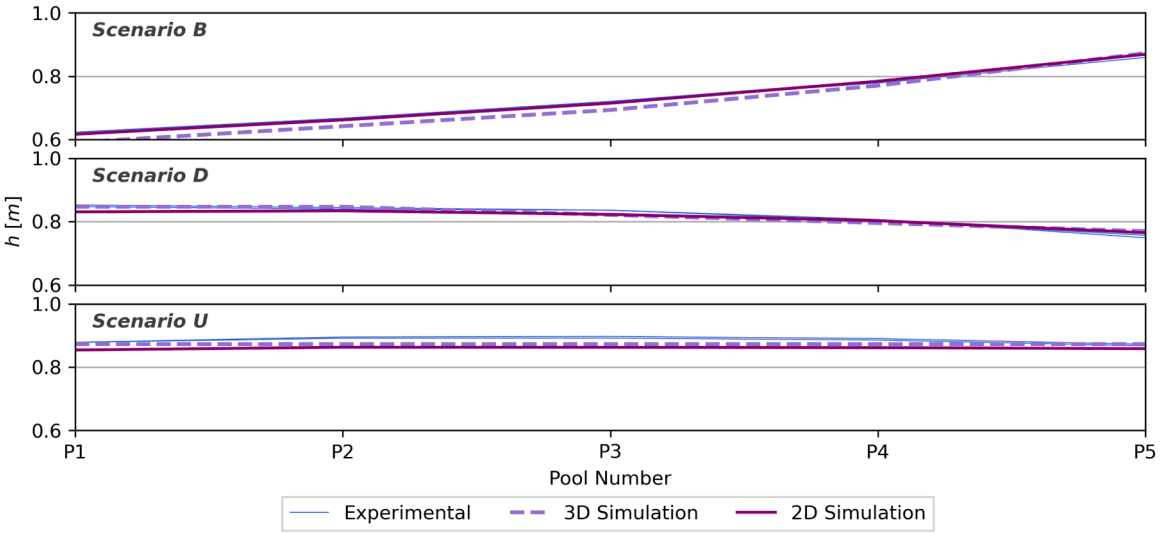

Fig. 4. Water depth variation along the pools of VSF_1 (Romão et al., 2017) observed by (Fuentes-Pérez et al., 2018), light blue lines, and simulated. Three – dimensional simulations are presented as light purple dashed lines, while two-dimensional simulations are presented as violet line. Free surface profiles from each scenario have been successfully reproduced by simulations.

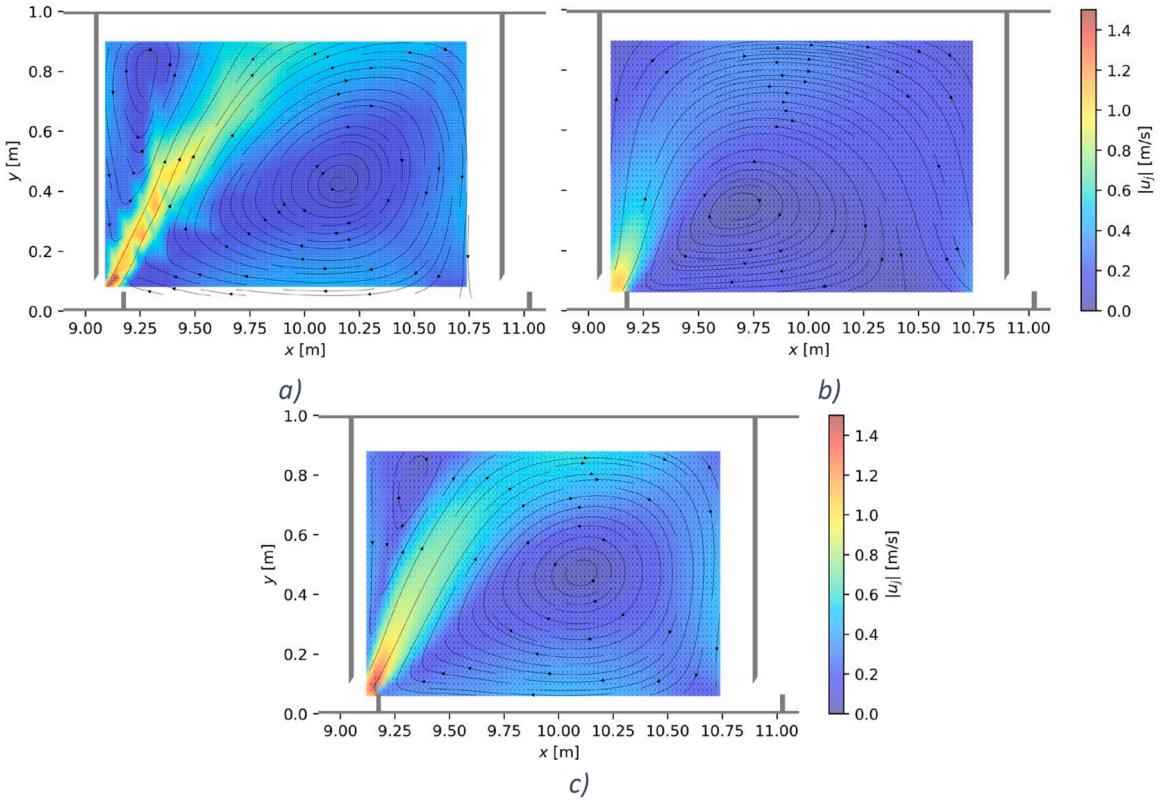

Fig. 5. Flow topology at the fifth pool of the VSF_1 at the Scenario U. The Fig. shows the density plot of the velocity magnitude for a) ADV measurements, b) 2D simulation and c) 3D simulation.

$$\frac{\Delta E}{\Delta t} = \frac{1}{2}\rho \cdot S \cdot C_D \cdot U_P{}^3 \tag{10}$$

where $\Delta E/\Delta t$ is the work done by the fish (agent), ρ is the water density, S is the wetted area from ideal surface of the fish body considering an ellipsoid of revolution linked to the fish Body Length, BL (a = BL and b= 0.25*BL), $C_D = 0.015$is the drag coefficient (Webb, 1975), and U_P is the fish relative velocity magnitude respect to the flow velocity. Moreover, our model displays the passage proportion, i.e. the agent's likelihood of passage success at each time step. This approach is based in the studies of Sanz-Ronda et al. (2015) on barbel survivor functions (Fig. 6; Eq. 11)

$$\ln(P_{pass}) = \frac{-e^{\ln(D_{max}) - 3.584 + 0.041\ BL\ -\ 1.028\ u_{flow}}}{0.342} \tag{11}$$

where D_{max} is defined as the maximum distance the agent should swim to reach the fishway exit, if no resting would be needed. Considering that the agent's suitable path is longer than the total fishway length, the

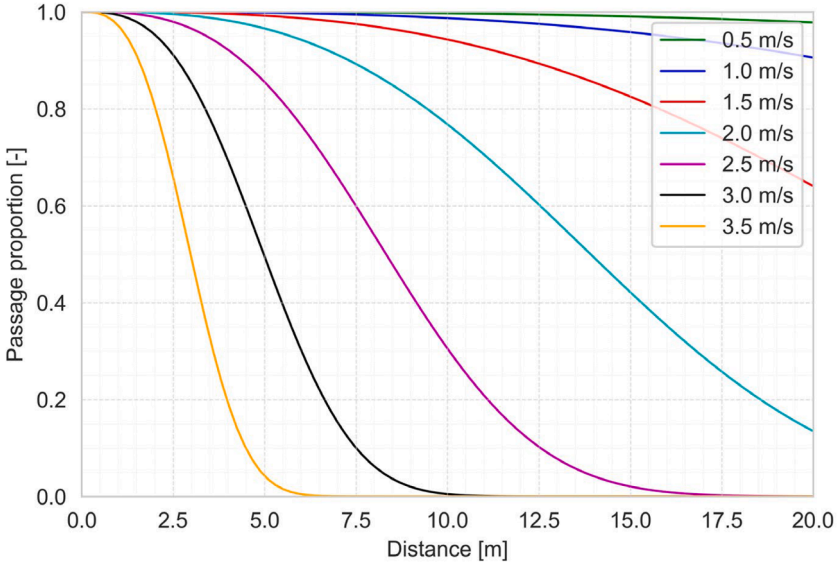

Fig. 6. Survival function or proportion of ascending as a function of the distance to the exist, a range of flow velocities, adapted from (Sanz-Ronda et al., 2015).

standard ELAM was run with the upstream migration and wall avoidance behaviors only. The results of these simulations are presented in Fig. 7. Then, a correction factor between the maximum path length and the fishway length was calculated $F = D_{max,ELAM}/L_{VSF}$, where $D_{max,ELAM}$ is the maximum length the agent covered and L_{VSF} is the horizontal length of the VSF. In this sense, we considered the ideal distance of the agent to reach the VSF's exit without resting. The factor F was 1.87, 1.81 and 1.84 for VFS_1, VFS_2 and VSF_3, respectively. Therefore, assuming that the fishway exit is at x-coordinate 0 and the VSF bottom is horizontal (with x as the main flow direction), $D_{max} = F^* x_{agent}$ in Eq. 11.

2.6. Dynamic simulation algorithm and dependencies (Telemac/TelApy)

The IBM was coded in Python 3.9 and coupled with TELEMAC-2D through the Application Programming Interface (API) TelAPy. The code runs for cases in which the VSF is horizontal, and the main flow direction is along the x-axis. The code collects previous TELEMAC-2D simulations and initializes the hydrodynamic model (h_0, $u_{i,0}$), and the IBM ($r_{fish,0}$, $u_{fish,0}$) parameters. h_0 and $u_{i,0}$ are the water depth and flow velocity at time t=0, while $r_{fish,0}$ and $u_{fish,0}$ are fish position and velocity at time t=0, respectively. The "standard ELAM" was the one developed by Ruiz-Coello et al. (2024a), and the fish body length for the simulations were set randomly to 0.2 m to 0.3 m, which is the reported in the studies of reference. Finally, as initial condition, time to fatigue, T_f, is set initially to ∞ and systematically decreases to 0.0 to reproduce fish exhaustion state. By introducing this condition, the time to fatigue will not be underestimated.

In order to correctly capture the ascent time, a data set of resting times linked to the likelihood of resting was built based on 1000 IBM simulations at VSF_1, VSF_2 and VSF_3. Contrary to the calibration simulations, the resting behavior was not activated but the triggering condition, $T_f = 0$, was counted. Table 2 shows the barbel's resting times linked to its probability of occurrence in the passage. While VSF_2 and VSF_3 shared similar times and probabilities, the barbel will rest at least twice in one passage, VSF_1 shows that the maximum resting events will be three times. The simulations including these values were performed again, with the resting behavior active for the validation process. A total of 68 agents were simulated, including 15 for VSF_1, 36 for VSF_2 and 17 for VSF_3, as in the experimental treatments. This data was finally validated with the total ascent times measured.

Contrary to the development of Ruiz-Coello et al., (2024a), the agent uses the sprint swimming speed only in the slot zone, neglecting it in the pool zone (Fig. 8). In addition, considering that the hydrodynamic time step, Δt, is much lower than the ELAM time step, Δt_{ELAM} the ELAM is computed when $\sum \Delta t \geq \Delta t_{ELAM}$. The algorithm constrains the domain, Ω_{ELAM}, to the pool in which the agent is located, unless, the agent is located in the slot zone, in which case the upstream pool is added for the analysis (Fig. 8). The outcome of the model includes all the behaviors described in Section 2.3, time to fatigue, passage proportion, energy expenditure, agent's position, and velocity. The flow chart of the t-ELAM-acPy_2D is presented in Figs. 9 and 10.

3. Results

The calibrated coefficients for upstream migration behavior (Eqs. 5 & 6) were the ones which minimized the maximum absolute error on frequency of use, *FU*, between experimental data and simulation results. *FU*was assessed in each block of the studied pool presented by Fuentes-Pérez et al. (2018) experiment. Considering that 3 scenarios were modelled and each scenario carries its own set of best coefficients, an average between the best coefficients was assumed. Table 3 shows the final coefficients for upstream migration behavior (Eqs. 5 & 6) for all the scenarios and the maximum absolute error of *FU*.

Table 4, on the other hand, displays the calibrated parameters on uncertainty and the best zone to trigger the resting behavior. Two evaluations were undertaken, because experimental measurements displayed two different preferred zones within scenarios according to Fuentes-Pérez et al., (2018). In the experiments performed by them, in the scenarios U and D, the barbels' behavior seems to be due to a resting action. On the other hand, in Scenario B it seems to be due to "seeking refuge" after finding the jet at the slot region. In our development though, we consider it as resting behavior.

We have taken the median of passage proportion from the pools 3, 4 for VSF_1 and 3, 4, 5 for VSF_2 and VSF_3 to contrast them with passage efficiency obtained with the experimental measurements. This is based on the fact that at least two pools are needed upstream and downstream to guarantee uniform flow in at least one of the pools (Ballu et al., 2019). In other words, we did not consider the influence of the inlet and outlet in the flow topology at the center of the fishway. Fig. 11 shows the 2D spatial distribution of the simulations after calibrating the resting times.

It is observed that the agent chooses the corners over the rest of the domain in VSF_1, while the preferred zone for resting in VSF_2 and VSF_3 is more spread. In this sense, it is observed that the model behaves differently in different geometries. After the final simulations,

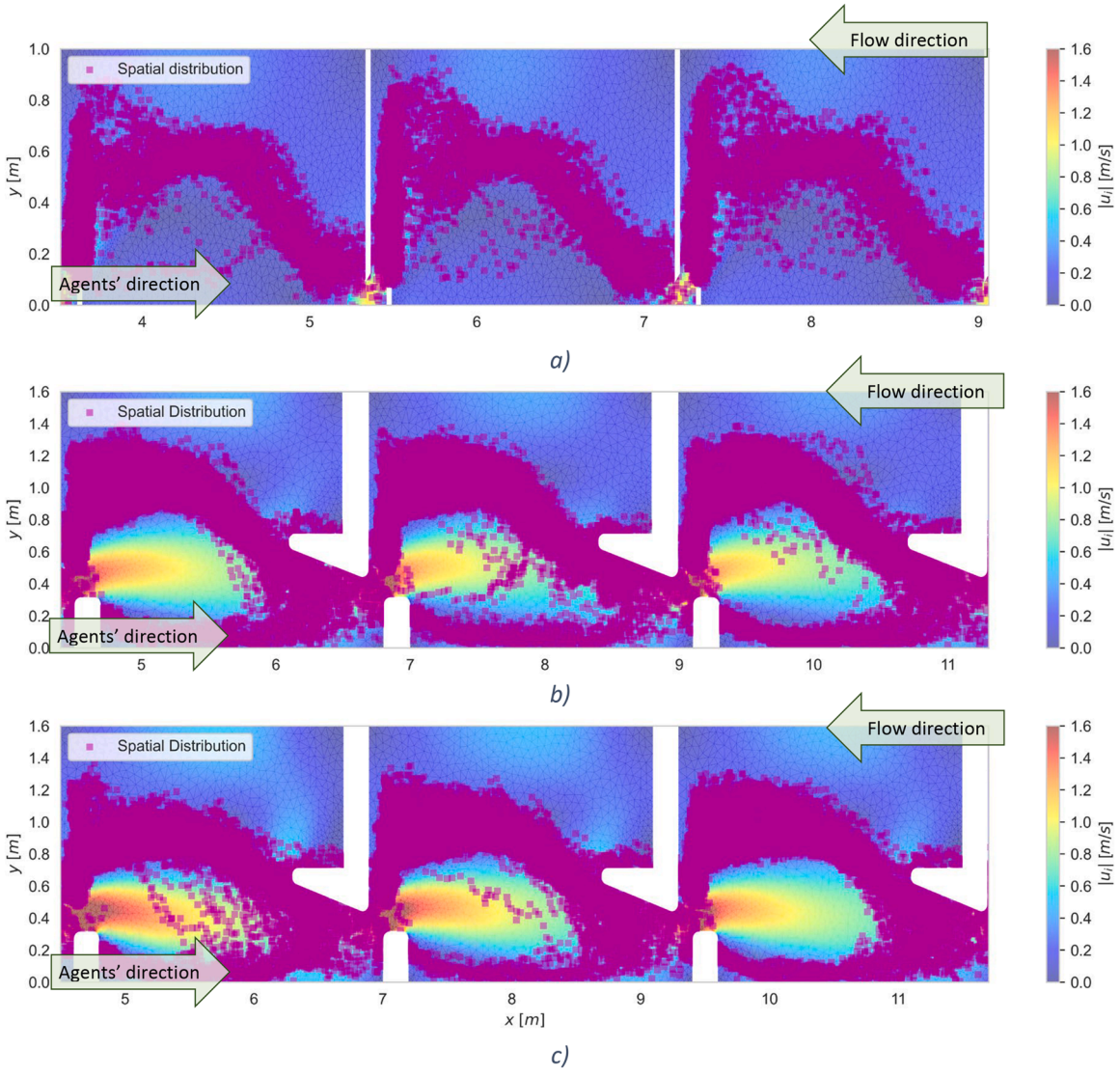

Fig. 7. Spatial distribution of fish locations obtained with the ELAM without the resting behavior, i.e., ideal agents' upstream migration path for the geometries a) VSF_1 (Romão et al., 2017), b) VSF_2 (Sanz-Ronda et al., 2019) and c) VSF_3 (Sanz-Ronda et al., 2016).

Table 2
Resting times of Iberian barbel for different geometries.

Resting Events	Case:	VSF_1: Romão et al., (2017)		VSF_2: Sanz-Ronda et al., (2019)		VSF_3: Sanz-Ronda et al., (2016)	
	Length:	12.75 m		16.10 m		16.60 m	
	Slope:	0.085 m/m		0.077 m/m		0.065 m/m	
		Time [s]	Probability [%]	Time [s]	Probability [%]	Time [s]	Probability [%]
1		924.25	27.25	-	-	-	-
2		462.13	57.00	350.71	12.90	415.13	8.85
3		308.08	15.75	233.81	45.81	276.75	44.16
4		-	-	175.36	24.52	207.56	37.00
5		-	-	140.28	14.19	166.05	8.17
6		-	-	116.90	2.58	138.38	1.82

experimental and simulated 2D spatial preferences were compared. Fig. 12 shows the 2D *FU* of the Iberian barbel and the agents' simulations regardless of the scenarios in pool 5 for the calibration geometry, VSF_1. The most used zone is the left corner downstream of the pool, which displayed*FU* of 0.36 and 0.40 in the experimental observations and the numerical simulations, respectively.

Fig. 13 shows the boxplots of the ascent time per meter of water drop (min/m), i.e. vertical height, distribution in the experimental measurements in comparison to those measured experimentally. Experimental outliers correspond to the 0.52% of the measurements. Therefore, we have neglected them in the boxplots for better understanding.

Romão et al. (2017) experimental data evaluation returns a median 15.3 min/m of ascent time for all scenarios, defined as the time elapsed

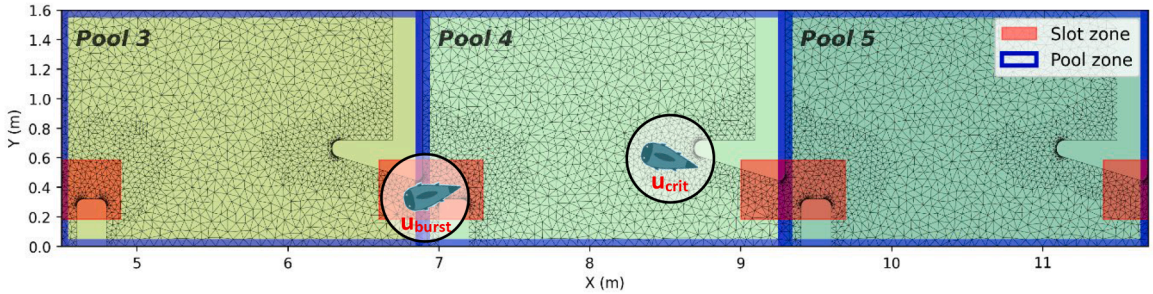

Fig. 8. Domain decomposition in t-ELAM-acPy_2D for the dynamic simulation ELAM and TELEMAC-2D. Only one pool is considered in the evaluation of the ELAM evaluation. If the agent is in the slot zone, adjacent pools are considered in the ELAM evaluation. In addition, when the agent is in the slot zone, the swimming speed is u_{burst} instead of u_{crit}.

between fish entry and exit of the fishway, while our model displayed 14.6 min/m (Fig. 13a). Their experimental data showed an ascent success, displayed an ascent success, computed as the proportion of individuals reaching the fishway exit, of 78.6 %. In comparison, our model displayed an average passage proportion of 93.2% (mean = 94.0%) in pools 3 and 4 (Table 5). (Sanz-Ronda et al., 2019) observed a median time of 6.9 min/m, while our model displayed 6.5 min/m (Fig. 13b). They published an ascent success of 94.9%, while our model displayed a median passage proportion of 85.6% (mean = 71.0%) ranged from pool 3 to 5 (Table 5). Finally, in the case of (Sanz-Ronda et al., 2016), agents were simulated under high, mean, and low flow conditions. While our model returned 8.30 min/m of ascent time, measurements displayed a median of 5.54 min/m (Fig. 13c). In this case the passage success for the Iberian barbel was around 71%, while our model displayed an average median of proportion of 91.0% (mean = 75.4%) ranged from pool 3 to 5 in the passage proportion. These values indicate that our model works well and can generalize between different VSF configurations and hydraulic conditions.

As shown in Table 5, the resting behavior slightly increases the passage proportion in the pools that are in the middle of the fishway, while it decreases when the pools are closer to the entrance or the exit. It is congruent with the fact that fish are more likely to succeed in passing the fishway if they are placed closer to the inlet. Fig. 14 shows the impact of resting behavior in the energy cost per unit of time.

The rate of energy spent per unit of time (Eq. 10) in the VSF1 geometry has a median of 1.65 cal/s (mean=1.77 cal/s) according to the standard ELAM, while with the resting behavior it is 0.58 cal/s (mean=0.62 cal/s). In the VSF2, geometry the median is 3.44 cal/s (mean=3.86 cal/s) according to the standard ELAM, whereas the addition of the resting behavior leads to a median of 7.72 cal/s (mean=7.57). In the VSF3, the median of the standard ELAM is 3.01 cal/s (mean=3.35 cal/s), as opposed to 3.85 cal/s (mean=5.24 cal/s) after including the resting behavior.

4. Discussion

Our proposal, t-ELAM-acPy_2D, has successfully coupled both fish swimming-migration models and hydrodynamic simulations in real time. The toolbox was built with the aid of open-source codes such as TELEMAC-2D and programing languages like Python 3.9. Thus, this development opens the branch of possibilities in the development of new tools in fish passage design and evaluation. While our models are focused on 2D hydrodynamic input and the fish species are cyprinids, the toolbox could be extended to a 3D approach and other targeted fish species, e.g. salmonids.

Based on experimental data, the Vertical Slot Fishway (VSF) is identified as a suitable type of fish passage structure for the Iberian barbel (Sanz-Ronda et al., 2016). In this sense depth-averaged simulations well reproduce velocities in the hydraulics of VSFs (Bombač et al., 2015; Chorda et al., 2010). We performed simulations following 2D and 3D approaches. The results were successfully contrasted against ADV measurements and well reproduced the water levels (Fig. 4). As shown in Fig. 5, the flow topology is not well captured by 2D simulations while the magnitude is similar. These results agree with those presented before in similar simulations (Ruiz-Coello et al., 2024c). The turbulence model used in this study, 2D $k-\varepsilon$ (Rastogi and Rodi, 1978), aims for the closure of the governing equations and does not predict the true k, instead it returns approximate values (Elgamal, 2022). Thus, turbulent variables such as Turbulent Kinetic Energy tend to be largely overestimated with respect to those in the 3D simulations.

Ruiz-Coello et al. (2024b) showed that, although 2D turbulent parameters are commonly and successfully used as input for IBM simulations, its influence on agents' cognitive responses tends to be biased from the real 3D approaches. To address this gap, the calibration of the IBM parameters took place for both 2D and 3D simulations. Table 3 shows that there are significant differences between the weights of each variable, as well as the differences between magnitudes of mean and standard deviation in k and $|S_{ij}|$, between 2D and 3D. These results agree with Ruiz-Coello et al. (2024b), who identified significant differences in $|S_{ij}|$ spatial distribution when 3D simulation was contrasted with 2D even though the overall values were similar. In the same line, previous studies have shown that $|S_{ij}|$ is of little or no significance in path selection (Ruiz-Coello et al., 2024a; Tan et al., 2019). In this case, $|S_{ij}|$ was not implemented as triggering parameter for agent's path selection in the 2D final implementation. Turbulent Kinetic Energy, k, is the most significant variable for both 2D and 3D path selection. This has been observed in previous studies (Liao, 2007; Silva et al., 2020, 2012). Velocity magnitude $|u_j|$ has similar meaning and standard deviation in both 2D and 3D simulations. Our results agree with the ones presented by Ruiz-Coello et al. (2024a)

Regarding the input of the model, the swimming performance of the Iberian barbel (*Luciobarbus bocagei*) is driven by a complex interplay of inherent biological traits and external hydrodynamic conditions. Barbels possess robustness and greater muscle mass per unit length compared to other cyprinids, enabling them to swim substantial distances in high-flow environments (Doadrio, 2001; Sanz-Ronda et al., 2016). Biological factors such as size influence swimming performance. Larger male individuals swim longer distances (Sanz-Ronda et al., 2015) compared to females and juveniles. Barbels are highly sensitive to the local flow environment and exhibit a strong preference for calm areas (Fuentes-Pérez et al., 2018). Our model correctly identified regions of low turbulence and velocity magnitude as suitable resting areas. However, despite accurately reproducing ascent times and frequency of use, t-ELAM-acPy_2D cannot capture the physiological differences among individuals, which are addressed by a random variable.

The uncertainties found in path selection in the 2D and 3D simulations are not consistent with each other. This may occur because the preferred blocks are at the bottom of the pool, so we can conclude that vertical movement is significant in resting behaviors. Furthermore, the best responses of the model are obtained when the behavior is triggered

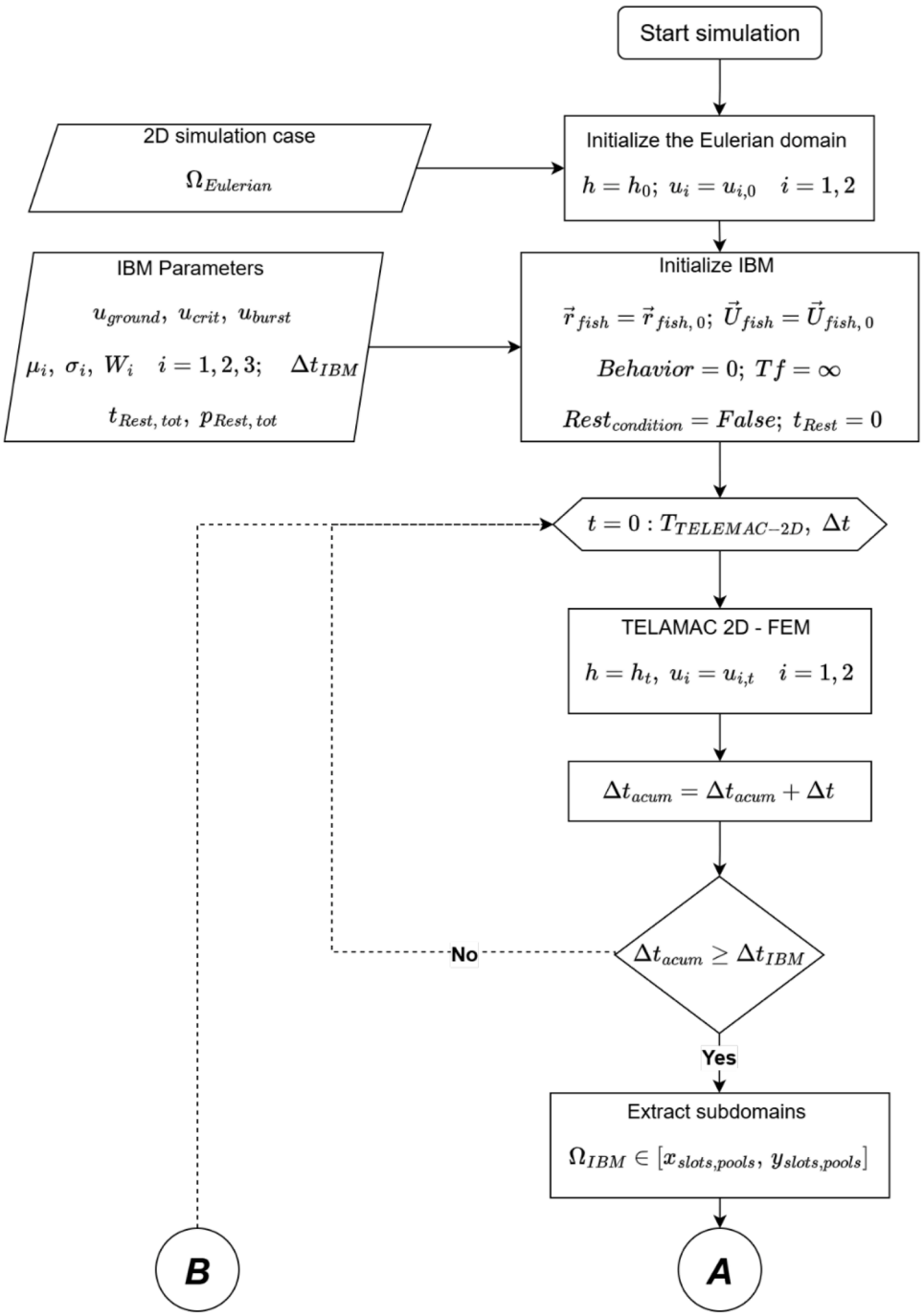

Fig. 9. First part of the t-ELAM-acPy_2d flow chart. At this stage of the algorithm, both the Hydrodynamic model and the Individual-based model are initialized. $\boldsymbol{h}$ and $\boldsymbol{u_i}$ are the water depth and velocity components. $\boldsymbol{\mu}$, $\boldsymbol{\sigma}$ and $\boldsymbol{W}$ are the coefficients to drive the standard IBM (Ruiz-Coello et al., 2024a), $\boldsymbol{\Delta t_{IBM}}$ is the time step of the IBM. Finally, $\boldsymbol{t_{rest,tot}}$ and $\boldsymbol{p_{rest,tot}}$, are the resting time and its likelihood obtained from Table 2. The loop for the resolution of the Eulerian framework starts and the controller $\boldsymbol{\Delta t_{acum}}$ sums all time steps until it is equal or larger than the IBM time step. If the condition is fulfilled, the IBM is simulated.

in the slot zone (within 10% of the pool length), whether upstream or downstream. In the 2D simulations the uncertainty of finding the best resting zone is lower in scenarios U and D than in scenario B. In all scenarios, resting behavior triggered in the slot zone produced the best results, a region where fish typically expend the most energy during upstream migration. Additionally, In the 3D simulation, the exploratory behavior triggered in scenario B displayed better results in the middle of the pool and the uncertainty was lower. Hence, it can be inferred that vertical movement in escaping or resting behavior may be crucial for similar 3D further developments.

During the validation process, ELAM simulation times increased by up to a factor of 48, which would be unfeasible and computationally prohibitive for three-dimensional ELAM implementations, even when parallelized. Therefore, the final toolbox was tested and validated for the 2D approach even though coefficients were calibrated for both 2D and 3D models. The simulations successfully reproduced median ascent time at the three VSF, in different hydrodynamic conditions. It is strongly suggested that, when suitable computational resources are available, the toolbox should be tested also in OpenFOAM or TELEMAC-3D. Katopodis and Kemp (2020) suggest using time resolved Particle Image Velocimetry (PIV) methods to achieve simultaneous measurements on fish responses and hydrodynamic data. ADV data, for example, cannot be

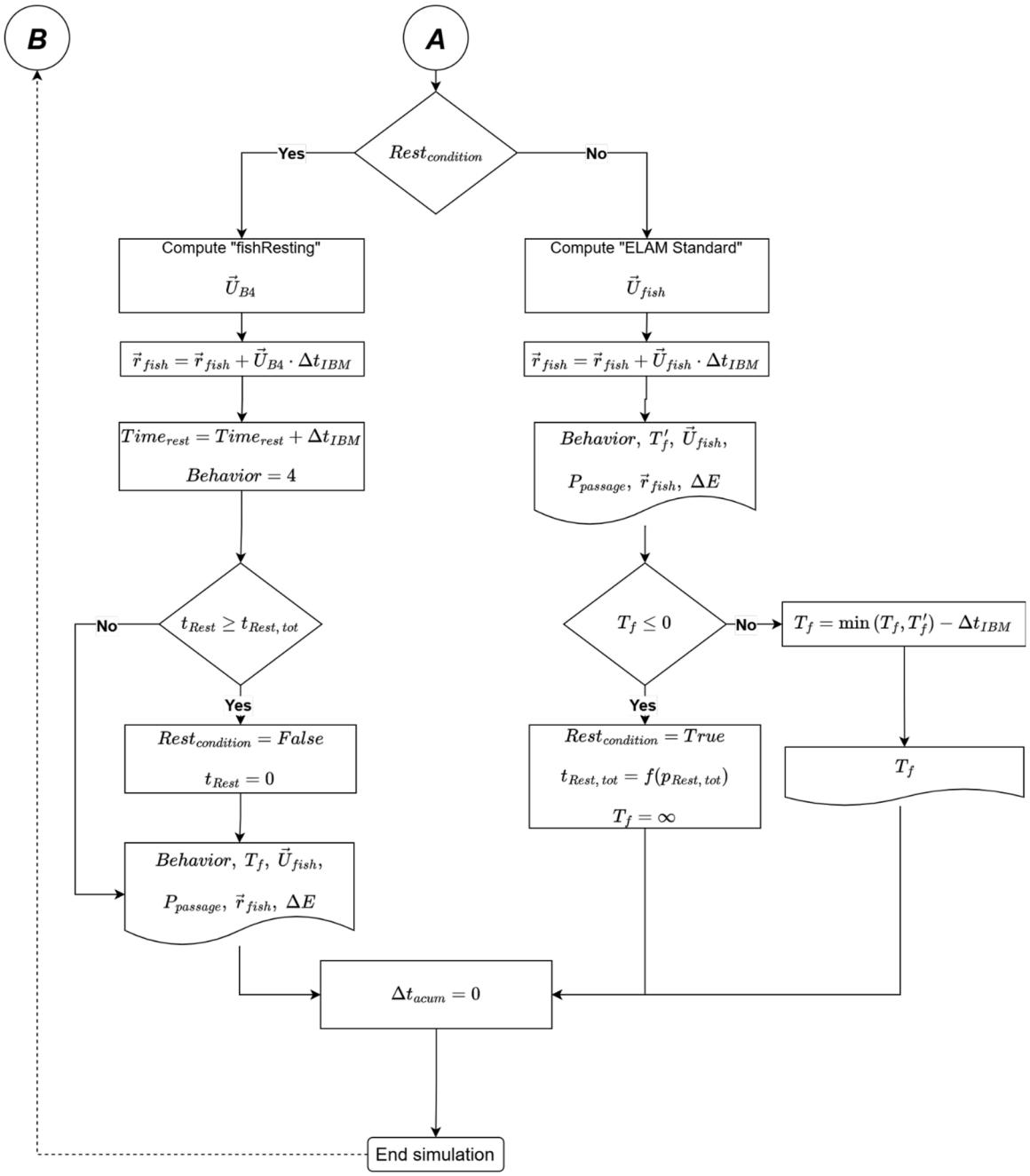

Fig. 10. Second part of the t-ELAM-acPy_2d flow chart. The Rest condition is evaluated to compute path preference and fish velocity, if false the ELAM standard (Ruiz-Coello et al., 2024a) is computed, $\vec{U}_{fish}$, if true the resting behavior is activated, $\vec{U}_{B4}$. In the first condition time to fatigue, T_f, decreases until it is zero. If T_f reaches down to zero, the rest condition is changed to "True". All the results are stored and Δt_{acum} is set to 0 to continue the hydrodynamic simulation. This process will continue until the iterations defined by the user are completed.

Table 3
Calibrated coefficients for upstream migration behavior.

Case	k			$\|u_j\|$			$\|S_{ij}\|$			Max Error FU (-)		
	μ (m^2/s^2)	σ(m^2/s^2)	W (-)	μ (m^2/s^2)	σ(m^2/s^2)	W(-)	μ (m^2/s^2)	σ(m^2/s^2)	W(-)	B	D	U
Experimental	0.0396	0.0431	-	0.282	0.106	-	-	-	-	-	-	-
2D	0.0391	0.0507	0.731	0.189	0.116	0.267	1.6445	2.0465	0.002	0.185	0.138	0.180
3D	0.0129	0.0125	0.662	0.191	0.108	0.211	37.852	28.216	0.127	0.150	0.227	0.103

accurately quantified because of sampling-frequency limitations (Ruonan et al., 2016). In the same line, while the native parallel capabilities of TELEMAC-2D are well-established for solving the hydrodynamic equations, there is a specific need for parallelization within the integrated Individual-Based Model (IBM) and the hybrid interface to manage the increased computational load.

Table 4
Threshold values of uncertainty triggering resting behavior.

	Scenario U, D		Scenario B		Max Error FU (-)		
Case	Uncertainty (-)	Zone	Uncertainty (-)	Zone	B	D	U
2D	0.15-0.25	Slot Zone Upstream	0.60-0.70	Slot Zone Downstream	0.152	0.101	0.210
3D	0.70-0.75	Slot Zone Upstream	0.25-0.30	Middle of the Pool	0.133	0.141	0.137

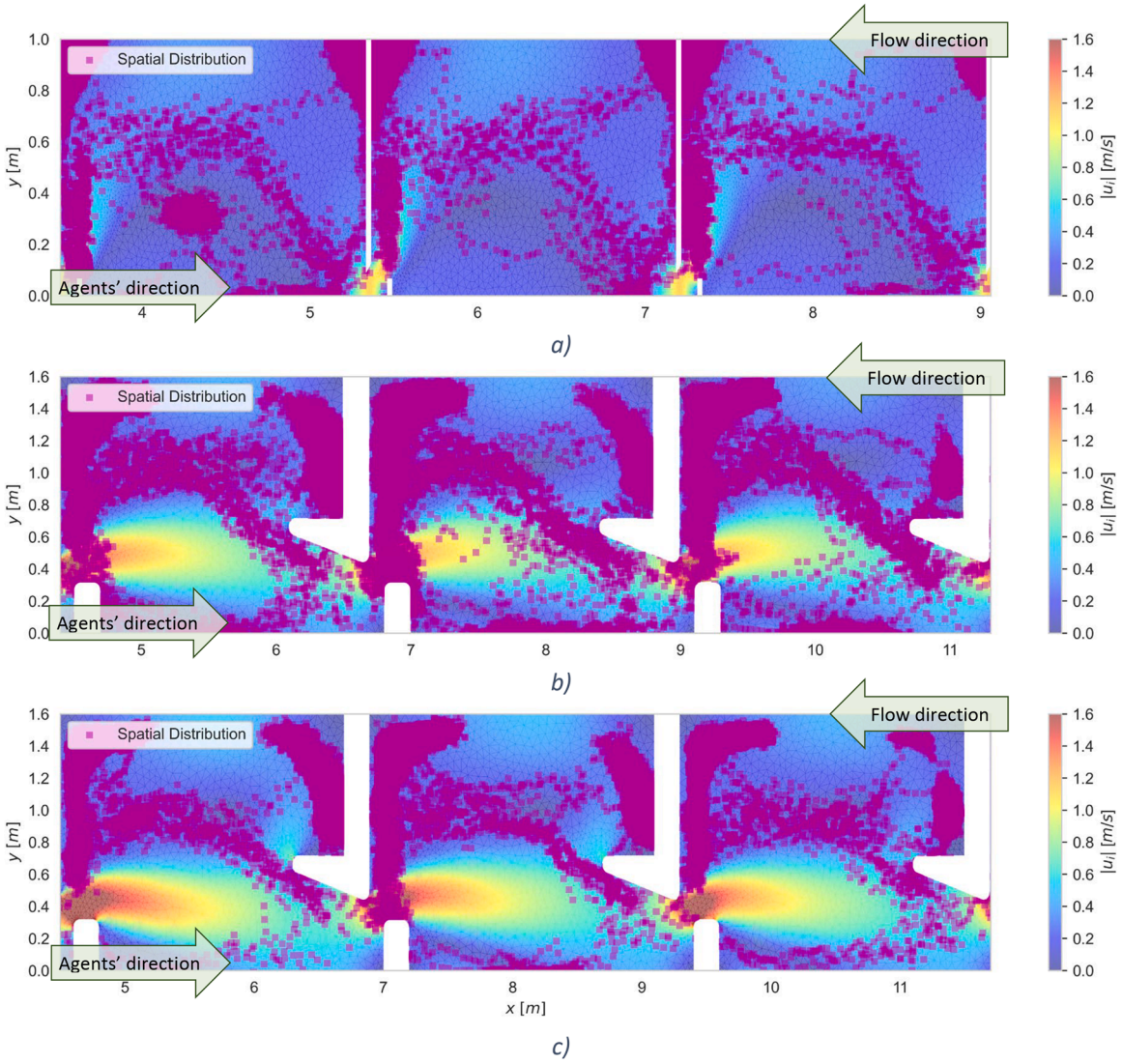

Fig. 11. Spatial distribution of fish instantaneous locations according to the ELAM simulations with resting behavior, i.e., modelled spatial preferences for the geometries a) VSF_1 (Romão et al., 2017), b) VSF_2 (Sanz-Ronda et al., 2019) and c) VSF_3 (Sanz-Ronda et al., 2016).

Calibration was based on the absolute error of the Frequency of Use, *FU*. In our simulations, this error was higher during the validation of upstream migration, as the experimental observations reported by Fuentes-Pérez et al. (2018) do not fully comply with the assumption of strictly upstream agent movement adopted by Ruiz-Coello et al. (2024a). Nonetheless, the available data reflects true barbel preferences linked to hydrodynamic cues. During calibration, the lowest error in 2D appeared in Scenario D, whereas in 3D it was Scenario U, consistent with results in Ruiz-Coello et al. (2024a). As shown in Fig. 12, *FU* in IBM simulations agrees with the measured one for the Iberian barbel. The zone most frequently occupied is the left corner downstream of the pool, which displayed *FU* of 0.36 and 0.40 in experimental and numerical results, respectively. The model did not capture *FU* of scenario B. Instead, the *FU* was higher in the upstream left corner of the pool away from the jet region, that might be suitable for resting since they are farthest from the jet.

In the validation process, the models reproduced median ascent times well, though variability in simulated distributions is lower. Simulated quartiles fall within experimental ranges for both ascent times and passage proportion, which was compared with passage efficiency. Even though the geometry used for validation (VSF_2 and VSF_3) has different hydrodynamic conditions compared with the geometry used for calibration (VSF_1), the validation parameters fall within acceptable ranges. Higher values of ascent time were measured in shorter distances. This is also reflected in energy consumption, as in the calibration geometry the energy cost is reduced significantly with the inclusion of the resting behavior, while the other two did not display any reduction. Instead, the energy cost increased. Implying that other variables might

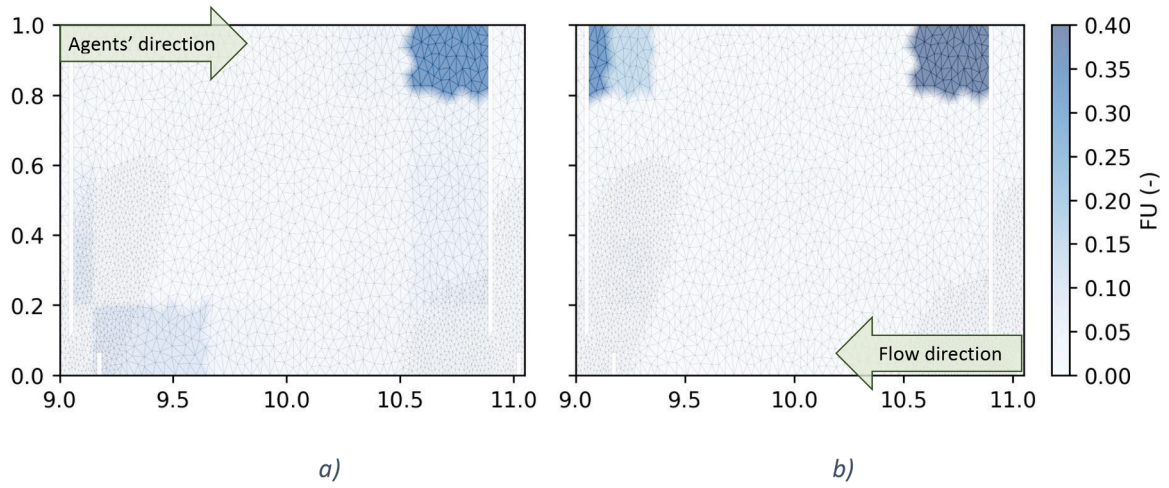

Fig. 12. 2D frequency of use of a) Iberian barbel (Fuentes-Pérez et al., 2018) and b) simulated by t-ELAM-acPy_2D.

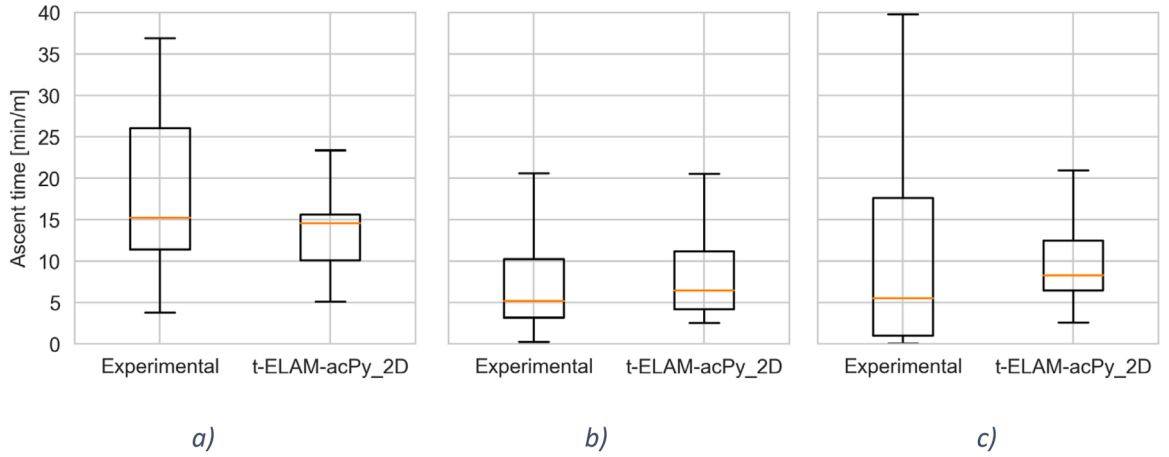

Fig. 13. Boxplot - distribution of ascent time per hydraulic water drop for a) VSF_1 (Romão et al., 2017), b) VSF_2 (Sanz-Ronda et al., 2019) and c) VSF_3 (Sanz-Ronda et al., 2016).

Table 5
Median of passage proportion of each case before and after adding resting behavior.

Case/Pool	Median of Passage Proportion						
	1	2	3	4	5	6	7
ELAM standard							
VSF_1	0.999	0.980	0.947	0.890	0.826	0.794	-
VSF_2	1.000	0.991	0.969	0.898	0.796	0.657	0.454
VSF_3	1.000	0.993	0.960	0.893	0.784	0.631	0.538
Resting Behavior							
VSF_1	0.999	0.995	0.956	0.907	0.866	0.683	-
VSF_2	0.999	0.991	0.954	0.914	0.701	0.649	-
VSF_3	0.999	0.995	0.956	0.907	0.866	0.683	-

interfere in energy recovery, rather than physical hydrodynamic parameters. Quantitative validation performed in previous studies (Chen et al., 2025; Gao et al., 2016; Ruiz-Coello et al., 2024a; Tan et al., 2018) was not suitable for the fishways presented in the manuscript. Since VSF_2 and VSF_3 are operating structures, upstream trajectories were not available. Nevertheless, the parameters used were found sufficient for this development.

The models tested in this paper are constrained. First, the hydraulics of VSF can be assumed two-dimensional at mild slopes (Bombač et al., 2015; Chorda et al., 2010). In this sense, the model could be used to evaluate nature-like fishways, whose slopes are generally mild, but will fail in evaluating submerged notch with bottom orifice fishways for instance. Second, different fish species would prioritize resting over other behaviors differently. Cyprinids, for example, rely more on resting in fish passage (Bravo-Córdoba et al., 2021), whereas salmonids exhibit higher swimming capabilities (Keefer et al., 2021) and therefore may require fewer resting events. Nevertheless, the results shown from the qualitative validation demonstrate that the inclusion of resting behavior increased the reliability of the simulations, at least for cyprinids.

The most relevant constraint to successfully model fish passage is the data availability for input and validation. While Katopodis and Gervais (2016) provide extensive swimming performance databases for calibration, future iterations could benefit from more detailed turbulent variable datasets (e.g., Reynolds Shear Stresses), which are currently scarce for targeted species. Nonetheless, although 2D models may overestimate turbulent kinetic energy compared to 3D models, our results confirm that the 2D approach offers an excellent balance between accuracy and computational efficiency. Finally, it is suggested exploring the reduction of the computational demands suggesting the need for parallelization or potential hybrid approaches with Machine Learning (Wang et al., 2023).

Summarizing, t-ELAM-acPy_2D toolbox represents the first of its kind capable of dynamically reproducing a wide range of cognitive swimming and migratory responses of cyprinid fish. It is an open-source complement built upon the free TELEMAC-2D code. The simulations are

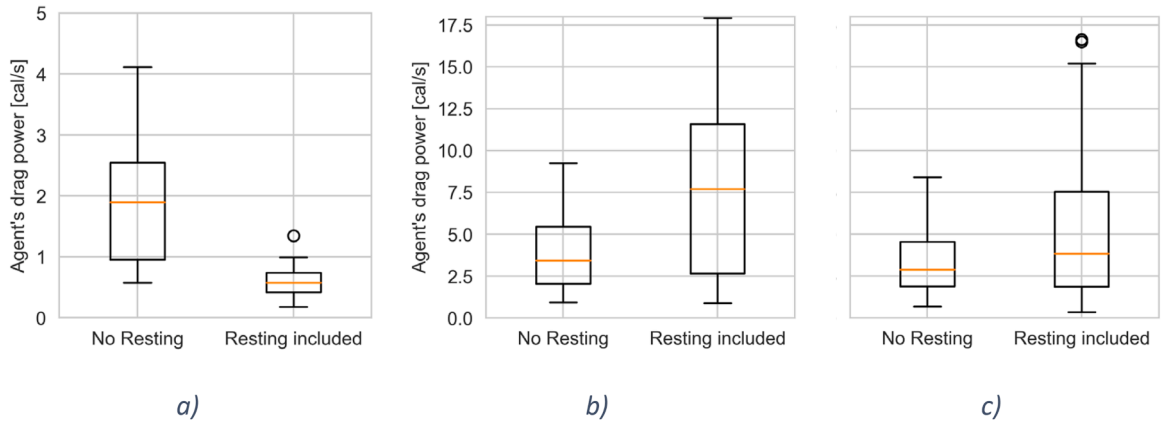

Fig. 14. Boxplot - distribution of Energy expenditure per unit of time a) VSF_1 (Romão et al., 2017), b) VSF_2 (Sanz-Ronda et al., 2019) and c) VSF_3 (Sanz-Ronda et al., 2016).

computationally efficient, requiring only modest runtimes, and allow the evaluation of transient, non-uniform flow conditions within vertical slot fishways. Although its primary development focuses on Vertical Slot Fishways (VSFs), the model can also be applied to natural riverine environments to analyze both upstream and downstream migrations of various target species. Non-hydrodynamic external and internal factors such as light, temperature, and stress, are represented through stochastic variables, while key biomechanical traits such as swimming capacity, fish length, and fatigue are explicitly accounted for. In summary, the model achieves a balance between accuracy and computational efficiency, even though certain biological factors remain simplified or excluded. It can be downloaded from the repository in Git-Hub, ELAM4VSF.

5. Conclusions

We presented a Eulerian Lagrangian Agent Based Model (ELAM) that can be coupled with TELAMAC – 2D (t-ELAM-acPy_2D) in a dynamic simulation using the API interface, TelApy. The ELAM theory is based on previously proposed model for Vertical Slot Fishways. However, in our new proposal we have included exploratory behavior linked to agent's exhaustion. The model has been calibrated for the Iberian Barbel (*Luciobarbus bocagei*), with experimental data in fish habitat preference. After calibration, the model was validated for two complex structures built in the Iberian Peninsula by comparing the ascent time distribution and fish passage efficiency.

Overall, t-ELAM-acPy_2D was able to reproduce fish upstream migration behavior under different conditions. The toolbox was coupled in real time simulation given the fish swimming models. Ascent times were successfully reproduced, and spatial distribution was fairly represented. Thus, it serves as a powerful instrument for the eco-hydraulic design and optimization of fish passage structures. Unlike traditional methods, this toolbox allows engineers and researchers to evaluate metrics such as energy expenditure, passage proportion or time-to-fatigue that are impossible to measure experimentally. Consequently, it enables the virtual testing of different VSF geometric configurations, allowing for the optimization of hydraulic steps and pool designs prior to construction. This predictive capability is essential for increasing passage efficiency and ensuring biological requirements are met cost-effectively.

In conclusion, the openly accessible t-ELAM-acPy_2D stands as a validated, physics-based tool. It provides a necessary bridge between hydraulic engineering and biology, offering a robust framework to assess and improve river connectivity solutions. Finally three-dimensional approaches, complex geometries and different fish species should be implemented in future research.

Software availability

The t-ELAM-acPy_2D model is an open-source tool developed in Python 3.9, coupled with TELEMAC-2D via the TelAPy API. The source code, documentation, and example cases used in this study are openly available at the GitHub repository ELAM4VSF and permanently archived at Zenodo with the identifier https://doi.org/10.5281/zenodo.17877818

CRediT authorship contribution statement

M.X. Ruiz-Coello: Writing – original draft, Visualization, Validation, Resources, Methodology, Investigation, Formal analysis, Data curation, Conceptualization. **F.J. Sanz-Ronda:** Writing – review & editing, Supervision. **A. Bottacin-Busolin:** Writing – review & editing, Validation, Supervision, Resources, Project administration, Conceptualization. **J.F. Fuentes-Pérez:** Writing – review & editing, Supervision, Software, Resources, Project administration, Funding acquisition, Data curation.

Declaration of competing interest

The authors declare that they have no known competing financial interests or personal relationships that could have appeared to influence the work reported in this paper.

Acknowledgments

This study was performed under the project "RIver flow regulation, fish BEhavior and Status (RIBES) framework". The project has received funding from the European Union Horizon 2020 Research and Innovation Programme under the Marie Sklodowska-Curie Actions, Grant Agreement No. 860800. The authors thank Prof. Andrea Marion for the funding acquisition in the first stage of this study. A broad set of experimental data was provided by the Applied Ecohydraulics Group (GEA) at the Univesidad de Valladolid for the calibration and validation of the present model. J.F. Fuentes-Pérez contribution was funded by the project RYC2022-036557-I funded by the Ministry of Science, Innovation and Universities, the Spanish Research Agency through the State Plan for Scientific, Technical and Innovation Research 2021-2023 (MCIU/AEI/10.13039/501100011033) and co-financed by the European Social Fund Plus (FSE+). Additional funding for this study was provided by the Junta de Castilla y León regional government (Spain) through project "CLU-2025-2-07 – iuFOR Institute Unit of Excellence" of the University of Valladolid, co-financed by the European Regional Development Fund (ERDF "Europe drives our growth")

Data availability

Data will be made available on request.

References

Ballu, A., Pineau, G., Calluaud, D., David, L., 2019. Experimental-based methodology to improve the design of vertical slot fishways. J. Hydraul. Eng. 145, 04019031. https://doi.org/10.1061/(ASCE)HY.1943-7900.0001621.

Belletti, B., Garcia de Leaniz, C., Jones, J., Bizzi, S., Börger, L., Segura, G., Castelletti, A., van de Bund, W., Aarestrup, K., Barry, J., Belka, K., Berkhuysen, A., Birnie-Gauvin, K., Bussettini, M., Carolli, M., Consuegra, S., Dopico, E., Feierfeil, T., Fernández, S., Fernandez Garrido, P., Garcia-Vazquez, E., Garrido, S., Giannico, G., Gough, P., Jepsen, N., Jones, P.E., Kemp, P., Kerr, J., King, J., Łapińska, M., Lázaro, G., Lucas, M.C., Marcello, L., Martin, P., McGinnity, P., O'Hanley, J., Olivo del Amo, R., Parasiewicz, P., Pusch, M., Rincon, G., Rodriguez, C., Royte, J., Schneider, C.T., Tummers, J.S., Vallesi, S., Vowles, A., Verspoor, E., Wanningen, H., Wantzen, K.M., Wildman, L., Zalewski, M., 2020. More than one million barriers fragment Europe's rivers. Nature 588, 436–441. https://doi.org/10.1038/s41586-020-3005-2.

Bombač, M., Četina, M., Novak, G., 2017. Study on flow characteristics in vertical slot fishways regarding slot layout optimization. Ecol. Eng. 107, 126–136. https://doi.org/10.1016/j.ecoleng.2017.07.008.

Bombač, M., Novak, G., Mlačnik, J., Četina, M., 2015. Extensive field measurements of flow in vertical slot fishway as data for validation of numerical simulations. Ecol. Eng. 84, 476–484. https://doi.org/10.1016/j.ecoleng.2015.09.030.

Bravo-Córdoba, F.J., Sanz-Ronda, F.J., Ruiz-Legazpi, J., Valbuena-Castro, J., Makrakis, S., 2018. Vertical slot versus submerged notch with bottom orifice: Looking for the best technical fishway type for Mediterranean barbels. Ecol. Eng. 122, 120–125. https://doi.org/10.1016/j.ecoleng.2018.07.019.

Bravo-Córdoba, F.J., Valbuena-Castro, J., García-Vega, A., Fuentes-Pérez, J.F., Ruiz-Legazpi, J., Sanz-Ronda, F.J., 2021. Fish passage assessment in stepped fishways: Passage success and transit time as standardized metrics. Ecol. Eng. 162, 106172. https://doi.org/10.1016/j.ecoleng.2021.106172.

Bunt, C.M., Castro-Santos, T., Haro, A., 2012. Performance of Fish Passage Structures at Upstream Barriers to Migration. River Res. Appl. 28, 457–478. https://doi.org/10.1002/rra.1565.

Cea, L., Pena, L., Puertas, J., Vázquez-Cendón, M.E., Peña, E., 2007. Application of several depth-averaged turbulence models to simulate flow in vertical slot fishways. J. Hydraul. Eng. 133, 160–172. https://doi.org/10.1061/(ASCE)0733-9429(2007)133:2(160).

Chen, X., Shi, X., Deng, X., Rasta, M., Tan, J., Wang, Y., Jiang, Y., Bai, Y., 2025. A multiple-behaviors virtual fish model for simulating fish trajectory in vertical slot fishways. J. Fish Biol. 106, 1899–1906. https://doi.org/10.1111/jfb.16064.

Chorda, J., Maubourguet, M.M., Roux, H., Larinier, M., Tarrade, L., David, L., 2010. Two-dimensional free surface flow numerical model for vertical slot fishways. J. Hydraul. Res. 48, 141–151. https://doi.org/10.1080/00221681003703956.

Doadrio, I., 2001. Atlas y Libro Rojo de los peces continentales. Consejo Superior de Investigaciones Científicas (CSIC), 1st ed. Ministerio del Medio Ambiente, Madrid, Spain.

Electricité de France, Sogreah, 2021. Hydraulic Research Wallingford, Centre D'etudes Techniques Maritimes Et Fluviales, Bundesanstalt Fur Wasserbau, Daresbury Laboratory, Artelia. TELEMAC-2D User Man.: Version v8p3 (User Manual No. v8p3). opentelemac.org. France.

Elgamal, M., 2022. A moment-based depth-averaged K-ε model for predicting the true turbulence intensity over bedforms. Water 14, 2196. https://doi.org/10.3390/w14142196.

European Commission, 2020. EU Biodiversity Strategy for 2030 (Communication), Bringing nature back into our lives. European Commission, Brussels, Belgium.

Fernandes, E.H., Dyer, K.R., Niencheski, L.F.H., 2001. Calibration and validation of the TELEMAC-2D model to the Patos lagoon (Brazil). J. Coast. Res 470–488.

Freyhof, J., Kottelat, M., 2008. Luciobarbus bocagei. IUCN Red List Threat. https://doi.org/10.2305/IUCN.UK.2008.RLTS.T2584A9458518.en. Species 2008, e. T2584A9458518.

Fuentes-Pérez, J.F., Eckert, M., Tuhtan, J.A., Ferreira, M.T., Kruusmaa, M., Branco, P., 2018. Spatial preferences of Iberian barbel in a vertical slot fishway under variable hydrodynamic scenarios. Ecol. Eng. 125, 131–142. https://doi.org/10.1016/j.ecoleng.2018.10.014.

Fuentes-Pérez, J.F., García-Vega, A., Sanz-Ronda, F.J., Paredes, A.M., de, A., 2017. Villemonte's approach: a general method for modeling uniform and non-uniform performance in stepped fishways. Knowl. Manag. Aquat. Ecosyst 23. https://doi.org/10.1051/kmae/2017013.

Gao, Z., Andersson, H.I., Dai, H., Jiang, F., Zhao, L., 2016. A new Eulerian–Lagrangian agent method to model fish paths in a vertical slot fishway. Ecol. Eng. 88, 217–225. https://doi.org/10.1016/j.ecoleng.2015.12.038.

Goeury, C., Audouin, Y., Zaoui, F., 2022. Interoperability and computational framework for simulating open channel hydraulics: application to sensitivity analysis and calibration of Gironde Estuary model. Env. Model. Softw. 148, 105243. https://doi.org/10.1016/j.envsoft.2021.105243.

Goodwin, R.A., Nestler, J.M., Anderson, J.J., Weber, L.J., Loucks, D.P., 2006. Forecasting 3-D fish movement behavior using a Eulerian–Lagrangian–agent method (ELAM). Ecol. Model. 192, 197–223. https://doi.org/10.1016/j.ecolmodel.2005.08.004.

Grill, G., Lehner, B., Thieme, M., Geenen, B., Tickner, D., Antonelli, F., Babu, S., Borrelli, P., Cheng, L., Crochetiere, H., Ehalt Macedo, H., Filgueiras, R., Goichot, M., Higgins, J., Hogan, Z., Lip, B., McClain, M.E., Meng, J., Mulligan, M., Nilsson, C., Olden, J.D., Opperman, J.J., Petry, P., Reidy Liermann, C., Sáenz, L., Salinas-Rodríguez, S., Schelle, P., Schmitt, R.J.P., Snider, J., Tan, F., Tockner, K., Valdujo, P. H., van Soesbergen, A., Zarfl, C., 2019. Mapping the world's free-flowing rivers. Nature 569, 215–221. https://doi.org/10.1038/s41586-019-1111-9.

Grizzetti, B., Pistocchi, A., Liquete, C., Udias, A., Bouraoui, F., van de Bund, W., 2017. Human pressures and ecological status of European rivers. Sci. Rep. 7, 205. https://doi.org/10.1038/s41598-017-00324-3.

Günther, A.C.L.G., 1868. Catalogue of the Fishes in the British Museum. British Museum (Natural History), Department of Zoology, London. https://doi.org/10.5962/bhl.title.8809.

Hershey, H., 2021. Updating the consensus on fishway efficiency: a meta-analysis. Fish Fish. 22, 735–748. https://doi.org/10.1111/faf.12547.

Katopodis, C., Gervais, R., 2016. Fish swimming performance database and analyses. Fisheries and Oceans Canada, Canada. https://publications.gc.ca/site/eng/9.810056/publication.html.

Katopodis, C., Kemp, P.S., 2020. Ecohydraulic flumes: are we taking full advantage of their potential for symmetrical interdisciplinary research? J. Ecohydraulics 5, 1–2. https://doi.org/10.1080/24705357.2020.1754553.

Keefer, M.L., Jepson, M.A., Clabough, T.S., Caudill, C.C., 2021. Technical fishway passage structures provide high passage efficiency and effective passage for adult Pacific salmonids at eight large dams. PLoS One 16, e0256805. https://doi.org/10.1371/journal.pone.0256805.

Kulić, T., Lončar, G., Kovačević, M., Fliszar, R., 2021. Application of agent-based modelling for selecting configuration of vertical slot fishway. Građevinar 73. https://doi.org/10.14256/JCE.3150.2021.

Liao, J.C., 2007. A review of fish swimming mechanics and Behaviour in altered flows. Philos. Trans. Biol. Sci. 362, 1973–1993.

Lucas, M.C., Baras, E., 2001. Migration or fresh water fishes. Blackwell Science, Oxford, UK.

McHenry, M.J., Liao, J.C., 2014. The Hydrodynamics of Flow Stimuli. In: Coombs, S., Bleckmann, H., Fay, R.R., Popper, A.N. (Eds.), The Lateral Line System, Springer Handbook of Auditory Research. Springer, New York, NY, pp. 73–98. https://doi.org/10.1007/2506_2013_13.

McKenzie, D.J., 2011. Swimming and Other Activities | Energetics of Fish Swimming. In: Farrell, A.P. (Ed.), Encyclopedia of Fish Physiology. Academic Press, San Diego, pp. 1636–1644. https://doi.org/10.1016/B978-0-12-374553-8.00151-9.

Puertas, J., Cea, L., Bermúdez, M., Pena, L., Rodríguez, Á., Rabuñal, J.R., Balairón, L., Lara, Á., Aramburu, E., 2012. Computer application for the analysis and design of vertical slot fishways in accordance with the requirements of the target species. Ecol. Eng. Ecohydraulic Approaches Restoring Habitat Connect. Suitabil. 48, 51–60. https://doi.org/10.1016/j.ecoleng.2011.05.009.

Rajaratnam, N., Katopodis, C., Solanki, S., 1992. New designs for vertical slot fishways. Can. J. Civ. Eng. https://doi.org/10.1139/l92-049.

Rastogi, A.K., Rodi, W., 1978. Predictions of heat and mass transfer in open channels. J. Hydraul. Div. 104, 397–420. https://doi.org/10.1061/JYCEAJ.0004962.

Romão, F., Quaresma, A.L., Branco, P., Santos, J.M., Amaral, S., Ferreira, M.T., Katopodis, C., Pinheiro, A.N., 2017. Passage performance of two cyprinids with different ecological traits in a fishway with distinct vertical slot configurations. Ecol. Eng. 105, 180–188. https://doi.org/10.1016/j.ecoleng.2017.04.031.

Ruiz-Coello, M.X., Bottacin-Busolin, A., Marion, A., 2024a. A Eulerian-Lagrangian model for simulating fish pathline distributions in vertical slot fishways. Ecol. Eng. 203, 107264. https://doi.org/10.1016/j.ecoleng.2024.107264.

Ruiz-Coello, M.X., Fuentes-Pérez, J.F., Sanz-Ronda, F.J., Marion, A., Bottacin-Busolin, A., 2024b. Suitability of 2D depth-averaged simulations to support predictions of cyprinids passage through Vertical Slot Fishways. J. Ecohydraulics 0, 1–14. https://doi.org/10.1080/24705357.2024.2363763.

Ruiz-Coello, M.X., Sandoval, R., Bottacin-Busolin, A., Guerra, M.J., Ríos, L., Ortega, P., Marion, A., 2024c. Numerical approaches to evaluate the hydraulics of vertical slot fishways: a comparative study of 2D and 3D simulations. In: Kalinowska, M.B., Mrokowska, M.M., Rowiński, P.M. (Eds.), Advances in Hydraulic Research. Springer Nature Switzerland, Cham, pp. 329–340. https://doi.org/10.1007/978-3-031-56093-4_26.

Ruiz-Legazpi, J., Sanz-Ronda, F.J., Bravo-Cordoba, F.J., Fuentes-Perez, J.F., Castro-Santos, T.R., 2018. Influencia de factores ambientales y biométricos en la capacidad de nado del barbo ibérico (Luciobarbus bocagei Steindachner, 1864), un ciprínido potamódromo endémico de la Península Ibérica. Limnetica. https://doi.org/10.23818/limn.37.21.

Ruonan, B., Liekai, C., Xingkui, W., Danxun, L., 2016. Comparison of ADV and PIV Measurements in Open Channel Flows. In: Procedia Eng., 12th International Conference on Hydroinformatics (HIC 2016) - Smart Water for the Future, 154, pp. 995–1001. https://doi.org/10.1016/j.proeng.2016.07.588.

Sanz-Ronda, F.J., Bravo-Córdoba, F.J., Fuentes-Pérez, J.F., Castro-Santos, T., 2016. Ascent ability of brown trout, Salmo trutta, and two Iberian cyprinids – Iberian barbel, Luciobarbus bocagei, and northern straight-mouth nase, Pseudochondrostoma duriense – in a vertical slot fishway. Knowl. Manag. Aquat. Ecosyst. 10. https://doi.org/10.1051/kmae/2015043.

Sanz-Ronda, F.J., Bravo-Córdoba, F.J., Sánchez-Pérez, A., García-Vega, A., Valbuena-Castro, J., Fernandes-Celestino, L., Torralva, M., Oliva-Paterna, F.J., 2019. Passage performance of technical pool-type fishways for potamodromous cyprinids: novel experiences in semiarid environments. Water 11, 2362. https://doi.org/10.3390/w11112362.

Sanz-Ronda, F.J., Ruiz-Legazpi, J., Bravo-Córdoba, F.J., Makrakis, S., Castro-Santos, T., 2015. Sprinting performance of two Iberian fish: Luciobarbus bocagei and Pseudochondrostoma duriense in an open channel flume. Ecol. Eng. 83, 61–70. https://doi.org/10.1016/j.ecoleng.2015.05.033.

Silva, A.T., Bærum, K.M., Hedger, R.D., Baktoft, H., Fjeldstad, H.-P., Gjelland, K.Ø., Økland, F., Forseth, T., 2020. The effects of hydrodynamics on the three-dimensional downstream migratory movement of Atlantic salmon. Sci. Total Env. 705, 135773. https://doi.org/10.1016/j.scitotenv.2019.135773.

Silva, A.T., Katopodis, C., Santos, J.M., Ferreira, M.T., Pinheiro, A.N., 2012. Cyprinid swimming behaviour in response to turbulent flow. Ecol. Eng. 44, 314–328. https://doi.org/10.1016/j.ecoleng.2012.04.015.

Silva, A.T., Lucas, M.C., Castro-Santos, T., Katopodis, C., Baumgartner, L.J., Thiem, J.D., Aarestrup, K., Pompeu, P.S., O'Brien, G.C., Braun, D.C., Burnett, N.J., Zhu, D.Z., Fjeldstad, H.-P., Forseth, T., Rajaratnam, N., Williams, J.G., Cooke, S.J., 2018. The future of fish passage science, engineering, and practice. Fish Fish. 19, 340–362. https://doi.org/10.1111/faf.12258.

Tan, J., Gao, Z., Dai, H., Yang, Z., Shi, X., 2019. Effects of turbulence and velocity on the movement behaviour of bighead carp (Hypophthalmichthys nobilis) in an experimental vertical slot fishway. Ecol. Eng. 127, 363–374. https://doi.org/10.1016/j.ecoleng.2018.12.002.

Tan, J., Liu, Z., Wang, Yu, Wang, Yuanyang, Ke, S., Shi, X., 2022. Analysis of movements and behavior of bighead carps (Hypophthalmichthys nobilis) considering fish passage energetics in an experimental vertical slot fishway. Animals 12, 1725. https://doi.org/10.3390/ani12131725.

Tan, J., Tao, L., Gao, Z., Dai, H., Shi, X., 2018. Modeling fish movement trajectories in relation to hydraulic response relationships in an experimental fishway. Water 10, 1511. https://doi.org/10.3390/w10111511.

Wang, J., Qie, Z., Li, G., Ran, Y., Wu, X., 2023. An efficient fish migration modeling method integrating the random forest and Eulerian–Lagrangian–agent method for vertical slot fishways. Ecol. Eng. 195, 107067. https://doi.org/10.1016/j.ecoleng.2023.107067.

Webb, P.W., 1975. Hydrodynamics and energetics of fish propulsion, Catalogue No. Fs 94-190. Fisheries and Marine Service Department of the Environmen, Ottawa, Canada.